

**NONLINEAR THIN-PLATE BENDING ANALYSES
USING THE HERMITE REPRODUCING KERNEL APPROXIMATION***

SATOYUKI TANAKA

*Department of Transportation and Environmental Systems, Hiroshima University,
4-1, Kagamiyama 1-chome, Higashi-Hiroshima 739-8527, Japan[†]
satoyuki@hiroshima-u.ac.jp[‡]*

SHOTA SADAMOTO

*Department of Transportation and Environmental Systems, Hiroshima University,
4-1, Kagamiyama 1-chome, Higashi-Hiroshima 739-8527, Japan[§]
d115754@hiroshima-u.ac.jp^{**}*

SHIGENOBU OKAZAWA

*Department of Transportation and Environmental Systems, Hiroshima University,
4-1, Kagamiyama 1-chome, Higashi-Hiroshima 739-8527, Japan^{††}
okazawa@hiroshima-u.ac.jp^{‡‡}*

Received (Day Month Year)

Revised (Day Month Year)

This study analyzed thin-plate bending problems with a geometrical non-linearity using the Hermite reproducing kernel approximation and sub-domain stabilized conforming integration. In thin-plate bending analyses, the deflections and rotations satisfy so-called Kirchhoff mode reproducing conditions. It is then possible to solve large deflection analyses of thin-plates, such as elastic buckling problems, with high accuracy and efficiency. Total Lagrangian method is applied to solve the geometrical non-linearity of the thin-plates' deflections and rotations. The Green-Lagrange strain and second Piola-Kirchhoff stress forms are adopted to represent the strains and stresses in the thin-plates. Mathematical formulation and some numerical examples are also demonstrated.

Keywords: Hermite reproducing kernel approximation, thin-plate bending problem, Kirchhoff-Love hypothesis, geometrical non-linearity, total Lagrangian method

* Typeset names in 8 pt Times Roman, uppercase. Use the footnote to indicate the present or permanent address of the author.

[†] State completely without abbreviations, the affiliation and mailing address, including country. Typeset in 8 pt Times Italic.

[‡] Typeset author e-mail address in single line.

[§] State completely without abbreviations, the affiliation and mailing address, including country. Typeset in 8 pt Times Italic.

^{**} Typeset author e-mail address in single line.

^{††} State completely without abbreviations, the affiliation and mailing address, including country. Typeset in 8 pt Times Italic.

^{‡‡} Typeset author e-mail address in single line.

1. Introduction

In recent years, Galerkin-based meshfree/particle methods have been proposed and developed to solve engineering problems. These include the Element-free Galerkin Method (EFGM) [Belytschko T. *et al.* (1994)], the Reproducing Kernel Particle Method (RKPM) [Liu W. K. *et al.* (1995)], and the Meshless Local Petrov-Galerkin (MLPG) method [Atluri S. N. *et al.* (1998)], etc. In solid/structural analyses using the meshfree/particle methods, the bodies are discretized based on the nodes/particles, and the deformations are represented by the interpolation functions which are located on the nodes/particles. The methodologies require no finite element meshes in the discretization and therefore avoid mesh distortion difficulties in large deformation analyses. When plate bending problems are solved using the meshfree/particle methods, there are some techniques required to make a structural element because the interpolation functions and the numerical integration of the stiffness matrices are sometime different from conventional finite element methods (FEMs). Some researchers have attempted to solve thin-plate structures using meshfree/particle methods; EFGM [Krysl P. and Belytschko T. (1995)] [Krysl P. and Belytschko T. (1996)], [Noguchi *et al.* (2000)], MLPG [Atluri S. N. *et al.* (1999)], and RKPM [Wang D. and Chen J. S., (2004)] [Chen J. S. and Wang D., (2006a)], etc.

The Hermite reproducing kernel (HRK) approximation with sub-domain stabilized conforming integration (SSCI) is one of the meshfree/particle methods to solve thin-plate bending problems [Wang D. and Chen J. S., (2008)]. The use of HRK approximation to the thin-plate bending problem, the deflections and the rotations, satisfy so-called Kirchhoff mode reproducing conditions. The rotations and the curvatures are directly represented by the differentiations of the deflection based on Hermite-type interpolation forms. Furthermore, the SSCI enhances the accuracy and numerical stability of the solutions in treating weak forms for thin-plate bending problems that have second-order differentiation of the deflection. The SSCI is based on stabilized conforming nodal integration (SCNI) proposed by Chen [Chen J. S. *et al.* (2001)] [Chen J. S. *et al.* (2002)]. In Galerkin-based meshfree/particle methods, a strain smoothing and stabilization of the solution can be achieved in performing numerical integration of the stiffness matrices with SCNI.

The goal of the research is to solve nonlinear analysis of thin-plates structures using HRK and SSCI as engineering applications. In this study, as a first attempt, the geometrical non-linearity using the total Lagrangian method is introduced to the thin-plate bending analyses. The Green-Lagrange strain and second Piola-Kirchhoff stress are used to represent the strains and stresses in the thin-plate. As far as we know, the development of thin-plate analyses using HRK and SSCI with geometrical non-linearity has not been presented to date. In addition, though Wang *et al.* used the mixed transformation method to enforce the essential boundary condition of the deflections and rotations [Chen J. S. and Wang H. P. (2000)], penalty formulation is adopted because it is easy to implement in the computer program without additional degrees of freedom to the system. In this paper, a review of thin-plate analyses with HRK and SSCI is briefly presented in Section

2. The methodology is expanded to the thin-plate bending analyses with geometrical non-linearity using the total Lagrangian method in Section 3. Some numerical examples of the thin-plate bending problem are demonstrated in Section 4, and compared with reference solutions using commercial FEM software to verify the developments. In Section 5, the conclusions of the present study are discussed.

2. Thin-Plate Bending Problem using the HRK Approximation and SSCI

In this section, a brief review for the thin-plate bending analyses using the HRK approximation with SSCI [Wang D. and Chen J. S., (2008)] is presented.

2.1. HRK approximation

The illustration for the thin-plate bending problem is shown in Fig. 1. In the analysis, Kirchhoff-Love hypothesis is assumed. The plate domain is Ω and the boundary is Γ . The plate thickness is t . The rotation θ_x and θ_y are defined as the illustration in Fig. 1. In Fig. 2, the schematic illustration for thin-plate bending analyses using the HRK approximation is presented. In the analyses, nodes are located in the mid-section of the plate. Each node has three degrees of freedom, i.e., deflection component and rotation components for the x -direction and y -direction. The deflection $w^h(\mathbf{x})$ at the position \mathbf{x} is represented by the superposition of the HRKs with their coefficients, as:

$$w^h(\mathbf{x}) = \sum_{I=1}^{NP} [\Psi_I^d(\mathbf{x})d_I^d + \Psi_I^{\theta_x}(\mathbf{x})d_I^{\theta_x} + \Psi_I^{\theta_y}(\mathbf{x})d_I^{\theta_y}] = \sum_{I=1}^{NP} \mathbf{\Psi}_I(\mathbf{x})\mathbf{d}_I \quad (1)$$

$$\mathbf{\Psi}_I(\mathbf{x}) = \left\{ \Psi_I^d(\mathbf{x}) \quad \Psi_I^{\theta_x}(\mathbf{x}) \quad \Psi_I^{\theta_y}(\mathbf{x}) \right\} \quad (2)$$

$$\mathbf{d}_I = \left\{ d_I^d \quad d_I^{\theta_x} \quad d_I^{\theta_y} \right\}^T \quad (3)$$

where $\Psi_I^d(\mathbf{x}) (I=1, \dots, NP)$ are the HRK for the deflection component, and $\Psi_I^{\theta_x}(\mathbf{x}), \Psi_I^{\theta_y}(\mathbf{x}) (I=1, \dots, NP)$ are the HRKs representing the rotation components for the x -direction and y -direction. $w_I, d_I^{\theta_x}, d_I^{\theta_y} (I=1, \dots, NP)$ are the coefficients. NP gives the total number of nodes in the support area. The HRKs $\Psi_I^d(\mathbf{x}), \Psi_I^{\theta_x}(\mathbf{x}), \Psi_I^{\theta_y}(\mathbf{x})$ for I -th node are represented by the superposition of the original kernel function $\phi_a(\mathbf{x})$. In this study, a cubic spline kernel function is adopted as the kernel function $\phi_a(\mathbf{x})$ given by,

$$\phi_a(\mathbf{x}_I - \mathbf{x}, a) = \frac{10}{7\pi h^2} \begin{cases} 1 - \frac{3}{2}s^2 + \frac{3}{4}s^3 & (0 \leq s \leq 1) \\ \frac{1}{4}(2-s)^3 & (1 \leq s \leq 2) \\ 0 & (2 \leq s) \end{cases} \quad s = \frac{|\mathbf{x}_I - \mathbf{x}|}{a} \quad (4)$$

in which s is the normalized distance and a is the radius of the kernel function. The HRKs are constructed by the sum of the kernel function $\phi_a(\mathbf{x})$ with the basis vectors $\mathbf{h}^T(\mathbf{x}_I - \mathbf{x}), \mathbf{h}_x^T(\mathbf{x}_I - \mathbf{x})$ and $\mathbf{h}_y^T(\mathbf{x}_I - \mathbf{x})$, as:

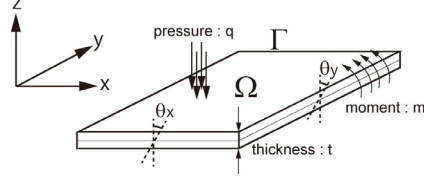


Fig. 1 Thin-plate Bending Problem

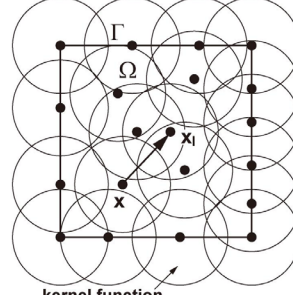


Fig. 2 Kernel Approximation

$$\begin{aligned}
 \Psi_I^d(\mathbf{x}) &= \mathbf{h}^T(\mathbf{x}_I - \mathbf{x}) \mathbf{b}(\mathbf{x}) \phi_a(\mathbf{x}_I - \mathbf{x}) \\
 \Psi_I^{\theta_x}(\mathbf{x}) &= \mathbf{h}_x^T(\mathbf{x}_I - \mathbf{x}) \mathbf{b}(\mathbf{x}) \phi_a(\mathbf{x}_I - \mathbf{x}) \\
 \Psi_I^{\theta_y}(\mathbf{x}) &= \mathbf{h}_y^T(\mathbf{x}_I - \mathbf{x}) \mathbf{b}(\mathbf{x}) \phi_a(\mathbf{x}_I - \mathbf{x})
 \end{aligned} \tag{5}$$

where $\mathbf{h}^T(\mathbf{x}_I - \mathbf{x})$ is the basis vector to represent the deflection component, and $\mathbf{h}_x^T(\mathbf{x}_I - \mathbf{x})$ and $\mathbf{h}_y^T(\mathbf{x}_I - \mathbf{x})$ are the basis vectors for the rotation components. Subscript a in kernel function $\phi_a(\mathbf{x}_I - \mathbf{x})$ is the function support. They are obtained by the differentiation of $\mathbf{h}^T(\mathbf{x}_I - \mathbf{x})$ for the x -direction and y -direction. In this study, second-order basis vectors are adopted and the vectors are represented as;

$$\begin{aligned}
 \mathbf{h}^T(\mathbf{x}) &= \{1 \quad x \quad y \quad x^2 \quad xy \quad y^2\} \\
 \mathbf{h}_x^T(\mathbf{x}) &= \frac{\partial \mathbf{h}(\mathbf{x})}{\partial x} = \{0 \quad 1 \quad 0 \quad 2x \quad y \quad 0\} \\
 \mathbf{h}_y^T(\mathbf{x}) &= \frac{\partial \mathbf{h}(\mathbf{x})}{\partial y} = \{0 \quad 0 \quad 1 \quad 0 \quad x \quad 2y\}
 \end{aligned} \tag{6}$$

In the HRK approximation, the coefficient vectors $\mathbf{b}(\mathbf{x})$ in Eq. (5) are determined to satisfy the n -th order reproducing conditions. The HRKs also satisfy the Kirchhoff mode reproducing condition. Further details for the derivation of the coefficient vectors and the Kirchhoff mode reproducing condition are presented in [Wang D. and Chen J. S. (2008)]. In Galerkin-based formulation for a thin-plate bending problem, curvature κ and the variation $\delta\kappa$ in the weak form are obtained directly by the second-order differentiation of deflection $w^h(\mathbf{x})$ and numerical integration is performed to determine the stiffness matrix. However, in the Galerkin-based meshfree/particle method, it is the possibility of stability deficiency in the solution occurring when the direct nodal integration or Gauss integration is performed. In this study, the SSCI is adopted to stabilize the solution.

2.2. Sub-domain stabilized conforming integration

The schematic illustration for SSCI is presented in Fig. 3. Though, it is known that the Voronoi diagram is often adopted for SSCI discretization, the geometric center surrounding the four nodes is used to make the integration cells a convenient means. In Fig. 3, the square region in the solid lines is the integration domain Ω_K for the K -th node. The region is divided into four sub-domains Ω_{Ki} ($i=1, \dots, 4$) to integrate the stiffness

matrix for the thin-plate bending problem accurately. The point \mathbf{x}_{K_i} is the geometric center of the sub-domain Ω_{K_i} where the physical values (strains, stresses, curvatures) are stored. In SSCI, smoothed curvatures at \mathbf{x}_{K_i} are represented as,

$$\begin{aligned} w_{\alpha\beta}^h(\mathbf{x}_{K_i}) &= \frac{1}{A_{K_i}} \int_{\Omega_{K_i}} w_{\alpha\beta}^h(\mathbf{x}) d\Omega_{K_i} \\ &= \frac{1}{2A_{K_i}} \int_{\Gamma_{K_i}} (w_{,\alpha}^h n_\beta + w_{,\beta}^h n_\alpha) d\Gamma_{K_i} \\ &= \frac{1}{2A_{K_i}} \sum_{I=1}^{NP} \left[\int_{\Gamma_{K_i}} \Psi_{I,\alpha}^j(\mathbf{x}_{K_i}) n_\beta d\Gamma_{K_i} d_I^j + \int_{\Gamma_{K_i}} \Psi_{I,\beta}^j(\mathbf{x}_{K_i}) n_\alpha d\Gamma_{K_i} d_I^j \right] \\ &\text{where } j = 1, 2, 3, \alpha, \beta = \{x, y\} \end{aligned} \quad (7)$$

where A_{K_i} is the area of Ω_{K_i} and n_α and n_β are normal vectors. The descriptions of the kernel function are represented as $\Psi_I^1(\mathbf{x}) \equiv \Psi_I^d(\mathbf{x})$, $\Psi_I^2(\mathbf{x}) \equiv \Psi_I^{\theta_x}(\mathbf{x})$, $\Psi_I^3(\mathbf{x}) \equiv \Psi_I^{\theta_y}(\mathbf{x})$, $d_I^1 \equiv d_I^d$, $d_I^2 \equiv d_I^{\theta_x}$ and $d_I^3 \equiv d_I^{\theta_y}$.

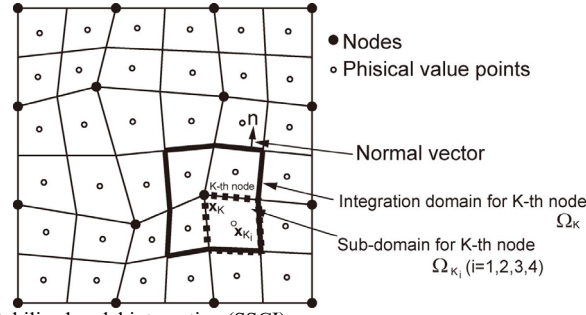


Fig. 3 Sub-domain stabilized nodal integration (SSCI)

3. Thin-plate bending problem with geometrical non-linearity

In this section, the thin-plate bending problem considering the geometrical non-linearity using the HRK approximation and SSCI are demonstrated.

3.1. Total Lagrangian method

The total Lagrangian method is adopted to solve the thin-plate bending problem with a geometrical non-linearity. The Green-Lagrange strain tensor and the second Piola-Kirchhoff stress tensor at time t for the initial configuration are represented as ${}^t_0\mathbf{E}$ and ${}^t_0\mathbf{S}$. The principle virtual work at time t without the body force term is represented as,

$$\int_{\Omega} {}^t_0\mathbf{S} : \delta_0 {}^t\mathbf{E} d\Omega - \int_{\Gamma_f} {}^t\bar{\mathbf{t}} \cdot \delta \mathbf{u} d\Gamma_f = 0 \quad (8)$$

in which $\delta \mathbf{u}$ is the variation of displacements \mathbf{u} , and ${}^t\bar{\mathbf{t}}$ is traction at the forced boundary Γ_f . To solve geometrical nonlinear bending problems, the principle virtual work in eq. (8) is decomposed and linearized. The principle virtual work at time $t+\Delta t$ is presented as,

$$\begin{aligned} & [\int_{\Omega} {}^t\dot{\mathbf{S}} : \delta_0' \mathbf{E} d\Omega + \int_{\Omega} {}^t\mathbf{S} : (\delta_0' \mathbf{E}) d\Omega] \Delta t \\ & \approx \int_{\Gamma_t} {}^{t+\Delta t} \bar{\mathbf{t}} \cdot \delta \mathbf{u} d\Gamma_t - \int_{\Omega} {}^t\mathbf{S} : \delta_0' \mathbf{E} d\Omega \end{aligned} \quad (9)$$

The upper script \bullet denotes the material time derivative. A penalty formulation is adopted to enforce the essential boundary condition for the deflections and rotations.

3.2. Implementation of the thin-plate bending problem

In the thin-plate bending problem considering the non-linear geometry, the linearized principle virtual work of Eq. (9) is used. In the matrix form for the left hand side of the equation is,

$$\text{Left hand side of Eq.(9)} = {}^t\mathbf{K}_L \mathbf{U} + {}^t\mathbf{K}_{NL} \mathbf{U} \quad (10)$$

$${}^t\mathbf{K}_L = \int_{\Omega} {}^t\mathbf{B}_L^T \mathbf{D} {}^t\mathbf{B}_L d\Omega \quad (11)$$

$${}^t\mathbf{K}_{NL} = \int_{\Omega} {}^t\mathbf{B}_{NL}^T {}^t\mathbf{S} {}^t\mathbf{B}_{NL} d\Omega \quad (12)$$

${}^t\mathbf{K}_L$ is the initial displacement matrix and ${}^t\mathbf{K}_{NL}$ is the geometric stiffness matrix. \mathbf{D} is the stress-strain relationship. Plane stress condition is assumed in this analysis. The integration of the plate thickness direction is performed analytically. The matrices ${}^t\mathbf{B}_{LI}$ for I -th particle are presented as,

$$\left\{ {}^tE_{11} \quad {}^tE_{22} \quad 2{}^tE_{12} \right\}^T = \sum_{I=1}^{NP} {}^t\mathbf{B}_{LI} \mathbf{U}_I \quad (13)$$

$${}^t\mathbf{B}_{LI} = \begin{bmatrix} B_{I11}^d & B_{I11}^{\theta_x} & B_{I11}^{\theta_y} \\ B_{I22}^d & B_{I22}^{\theta_x} & B_{I22}^{\theta_y} \\ B_{I12}^d & B_{I12}^{\theta_x} & B_{I12}^{\theta_y} \end{bmatrix} \quad (14)$$

where \mathbf{U}_I is displacement vector for I -th particle, and the components $B_{I\alpha\beta}^d$, $B_{I\alpha\beta}^{\theta_1}$, $B_{I\alpha\beta}^{\theta_2}$ $\{\alpha, \beta = 1, 2\}$ represent integration form with SSCI as:

$$\begin{aligned} B_{I\alpha\beta}^k &= -\frac{1}{2} \{ z b_{I\alpha\beta}^k + z b_{I\beta\alpha}^k + {}^t w_{,\alpha} b_{I\beta}^k + {}^t w_{,\beta} b_{I\alpha}^k \}, \\ b_{I\alpha\beta}^k &= \frac{1}{A_{K_i}} \int_{\Gamma_{K_i}} \Psi_{I,\alpha}^k n_{\beta} d\Gamma, \\ b_{I\beta}^k &= \frac{1}{A_{K_i}} \int_{\Gamma_{K_i}} \Psi_I^k n_{\beta} d\Gamma, \quad \text{where } \{\alpha, \beta = 1, 2\}, k = \{d, \theta_x, \theta_y\} \end{aligned} \quad (15)$$

For nonlinear part of Green-Lagrange strain ${}^t\mathbf{B}_{NLI}$ for I -th particle and second Piola-Kirchhoff stresses ${}^t\mathbf{S}$ are represented as,

$$\left\{ \frac{\partial^t w}{\partial x_1} \quad \frac{\partial^t w}{\partial x_2} \right\}^T = \sum_{I=1}^{NP} {}^t\mathbf{B}_{NLI} \mathbf{U}_I \quad (16)$$

$${}^t\mathbf{B}_{NL} = \begin{bmatrix} b_{I1}^d & b_{I1}^{\theta_x} & b_{I1}^{\theta_y} \\ b_{I2}^d & b_{I2}^{\theta_x} & b_{I2}^{\theta_y} \end{bmatrix}, \quad {}^t\mathbf{S} = \begin{bmatrix} {}^tS_{11} & {}^tS_{12} \\ {}^tS_{21} & {}^tS_{22} \end{bmatrix} \quad (17)$$

The right hand side of Eq. (9) is represented in matrix form as,

$$\text{Right hand side of Eq.(9)} = {}^{t+\Delta t}{}^0\mathbf{F} - {}^t{}^0\mathbf{Q} \quad (18)$$

${}^{t+\Delta t}{}^0\mathbf{F}$ is the external force vector for the pressure distribution and moments and ${}^t{}^0\mathbf{Q}$ is the internal force vector. The vectors can be written as follows:

$${}^{t+\Delta t}{}^0\mathbf{F} = \int_{\Gamma} \mathbf{N}^T {}^{t+\Delta t}{}^0\bar{\mathbf{t}} d\Gamma \quad (19)$$

$${}^t{}^0\mathbf{Q} = \int_{\Omega} {}^t\mathbf{B}_{L0}^T {}^t\hat{\mathbf{S}} d\Omega \quad (20)$$

in which ${}^t\hat{\mathbf{S}}$ is the vector form of ${}^t\mathbf{S}$. Numerical integration is performed using the SSC1 in Subsection 2.3 to stabilize the solution. To solve the linearized nonlinear equation from time t to $t+\Delta t$, incremental analyses are performed using the Newton-Raphson iteration method. The convergence is checked each increment step by step, and the iterations are finished when difference between the internal and external forces at the time $t+\Delta t$ is less than a threshold.

4. Numerical Examples

Numerical examples for thin-plate bending problem are demonstrated to verify the proposed technique. The thin-plate bending problem is shown in Fig. 4 (a) and (b). A 1000x1000 mm rectangular plate (plate thickness $t = 10$ mm) is used. The Young's modulus is $E = 206$ GPa and Poisson's ratio $\nu = 0.3$. Initial deflection is not considered. For the applied loads, the pressure distribution in Fig. 4 (a) and the point load at the center node in Fig. 4 (b) are applied. Two kinds of node distribution models are used in the analyses. Fig. 5 (a) shows the regular node model (21x21 nodes) and Fig. 5 (b) shows the irregular node model (21x21 nodes). The solutions are compared with the reference solution using MSC.MARC. A 100x100 elements model is used to model the plate and a thin-plate shell element (element number 139 in MSC. MARC) is adopted. As membrane deformation is not considered in this study, the degrees of freedom for the x , y deformations are fixed in the analyses with MSC.MARC. As the boundary condition, simply supported and clamped plate conditions are enforced along the edges of the plates. The numerical results are shown in Fig. 6 (a) and (b) for simply supported boundary condition. Cases for clamped plate condition are shown in Fig. 7 (a) and (b). In the figures, the deflections of center the plate are denoted. Both solutions for the regular node model and irregular node model are good agreement with the reference solution.

To perform further results evaluations, L_2 error norm is estimated for the thin-plate bending problems. Three kinds of analysis models with regular node pattern are used. They have 11x11, 21x21 and 41x41 nodes in each model, respectively. Final step deflections in Fig. 6 (a), (b) and Fig. 7 (a), (b) are used to compare the L_2 error norm for simply supported and clamped plate boundary conditions. Numerical results with

MSC.MARC are used as the reference solution. The numerical results under pressure distribution are shown in Fig. 8 (a) and under point load are presented in Fig. 8 (b). In both cases, the L_2 error norm are converged as the distance between nodes are closer. From the numerical results, it is considered that the proposed method can solve with high accuracy the thin-plate bending problem with geometrical non-linearity.

5. Conclusion

In this study, thin-plate bending problems with geometrical non-linearity are performed using the HRK approximation and SSCI. The total Lagrangian method is used to treat the non-linearity. Some numerical examples are presented to verifying the proposed method. For future study, a shell element formulation is to be developed considering membrane deformation using this technique and elastic bucking problems are solved for engineering applications.

Acknowledgement

Authors would like to express appreciation for the financial support of the SUZUKI FOUNDATION.

References

- Atluri S. N. and Zhu T., (1998). A new meshless local Petrov-Galerkin (MLPG) approach in computational mechanics, *Computational Mechanics*, **22**: pp. 117-127.
- Atluri, S. N., Cho, J. Y., Kim, H. G., (1999). Analysis of thin beams, using the meshless local Petrov-Galerkin method, with generalized moving least squares interpolations, *Computational Mechanics*, **24**: pp. 334-347.
- Belytschko T., Lu Y. Y. and Gu L., (1994). Element-free Galerkin Methods, *International Journal for Numerical Methods in Engineering*, **37**: pp. 229-256.
- Chen J. S., Wang D., (2006a). A constrained reproducing kernel particle formulation for shear deformable shell in Cartesian coordinates, *International Journal for Numerical Methods in Engineering*, **68**: pp. 151-172.
- Chen J. S., Wu C. T., Yoon S., You Y., (2001). A stabilized conforming nodal integration for Galerkin meshfree methods, *International Journal for Numerical Methods in Engineering*, **50**: pp. 435-466.
- Chen J. S., Yoon S., Wu C. T., (2002). Non-linear version of stabilized conforming nodal integration for Galerkin mesh-free methods, *International Journal for Numerical Methods in Engineering*, **53**: pp. 2587-2615.
- Chen J. S., Wang H. P., (2000). New boundary condition treatments for meshless computation of contact problems, *Computer Methods in Applied Mechanics and Engineering*, **187**: pp. 441-468.
- Krysl P., Belytschko T., (1995). Analysis of thin plates by the element-free Galerkin method, *Computational Mechanics*, **17**: pp. 26-35.
- Krysl P., Belytschko T., (1996). Analysis of thin shells by the element-free Galerkin method, *International Journal of Solids and Structures*, **33**: pp. 3057-3080.
- Liu W. K., Jun S., Zhang Y F., (1995). Reproducing kernel particle methods, *International Journal for Numerical Methods in Fluids*, **20**: pp. 1081-1106.
- Noguchi H., Kawashima T., Miyamura T., (2000). Element free analyses of shell and spatial structures, *International Journal for Numerical Methods in Engineering*, **47**: pp. 1215-1240.

- Wang D., Chen J. S., (2004), Locking-free stabilized conforming nodal integration for meshfree Mindlin-Reissner plate formulation, *Computer Methods in Applied Mechanics and Engineering*, **193**: pp.1065-1083.
- Wang D., Dong S. B., Chen J. S., (2006b). Extended meshfree analysis of transverse and inplane loading of a laminated anisotropic plate of general planform geometry, *International Journal of Solids and Structures*, **43**: pp. 144-171.
- Wang D., Chen J. S., (2008). A Hermite reproducing kernel approximation for thin-plate analysis with sub-domain stabilized conforming integration, *International Journal for Numerical Methods in Engineering*, **74**: pp. 368-390.
- Wang D., Lin Z., (2010). Free vibration analysis of thin plates using Hermite reproducing kernel Galerkin meshfree method with sub-domain stabilized conforming integration, *Computational Mechanics*, **46**: pp. 703-719.
- Zienkiewics O.C., Taylor R. L., (2005). The finite element method: for solid and structural mechanics 6th edition, Butterworth Heinemann.

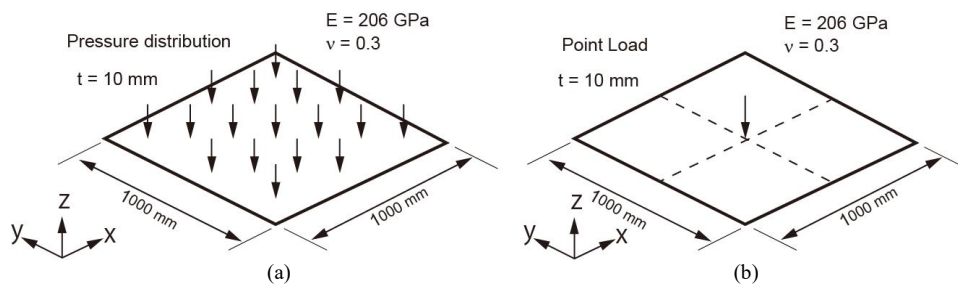


Fig. 4 Thin-plate bending analyses with geometrical non-linearity [(a) under pressure distribution, (b) under point load]

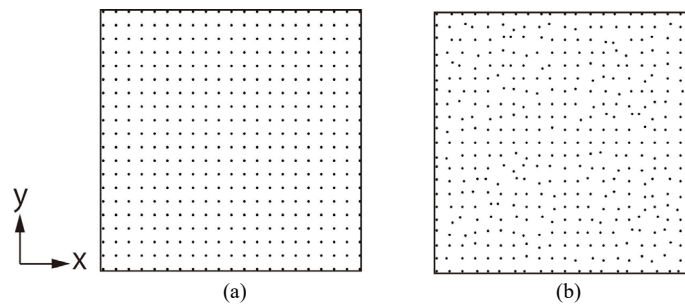


Fig. 5 Node distribution for the analyses of HRK with SSCI [(a) 21x21 regular nodes model, (b) 21x21 irregular nodes model]

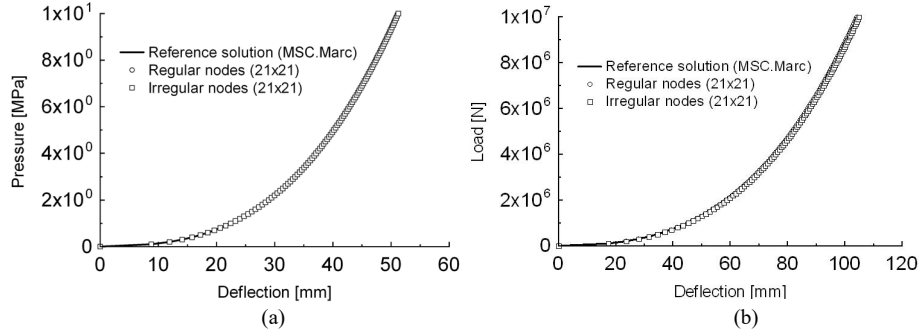


Fig. 6 Load-deflection curves (simply supported) [(a) Pressure distribution, (b) Point load]

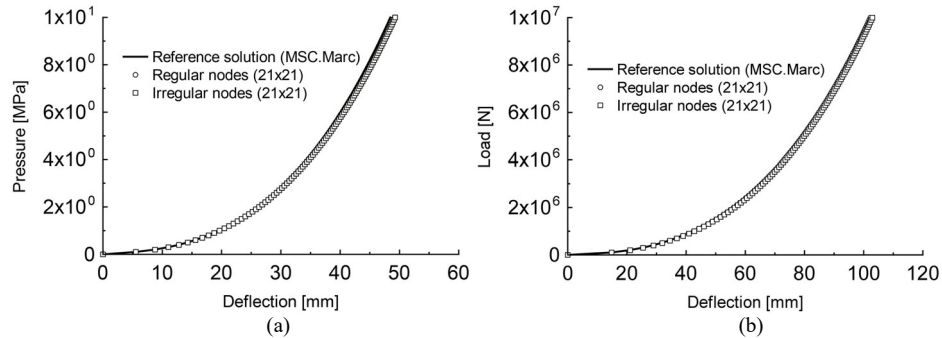


Fig. 7 Load-deflection curves (clamped plate) [(a) Pressure distribution, (b) Point load]

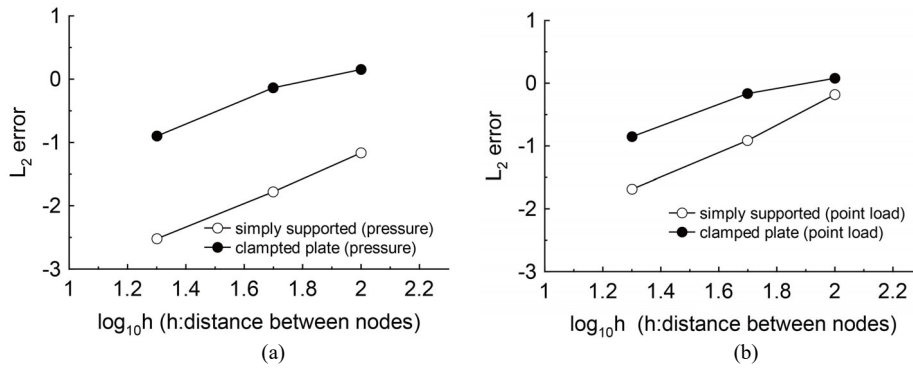


Fig. 8 L_2 error norm [(a) Pressure distribution, (b) Point load]